

Cite as: J. Vac. Sci. Technol. A 41, 023405 (2023); https://doi.org/10.1116/6.0002227 Submitted: 14 September 2022 • Accepted: 17 January 2023 • Published Online: 16 February 2023

Yifei Li, 🗓 Kate Reidy, 🗓 Aubrey Penn, et al.

COLLECTIONS

Paper published as part of the special topic on Thin Film Deposition for Materials Discovery



This paper was selected as an Editor's Pick







ARTICLES YOU MAY BE INTERESTED IN

Applications and mechanisms of anisotropic two-step Si₃N₄ etching with hydrogen plasma conditioning

Journal of Vacuum Science & Technology A 41, 022601 (2023); https://doi.org/10.1116/6.0002139

Molecular beam epitaxy of KTaO3

Journal of Vacuum Science & Technology A 41, 022703 (2023); https://doi.org/10.1116/6.0002223

On the limitations of thermal atomic layer deposition of InN using ammonia Journal of Vacuum Science & Technology A 41, 020401 (2023); https://doi.org/10.1116/6.0002355







Cite as: J. Vac. Sci. Technol. A 41, 023405 (2023); doi: 10.1116/6.0002227 Submitted: 14 September 2022 · Accepted: 17 January 2023 · Published Online: 16 February 2023







Yifei Li,¹ Kate Reidy,¹ D Aubrey Penn,² Seng Huat Lee,^{3,4} D Baoming Wang,¹ Kevin Ye,¹ D Zhiqiang Mao,^{3,4} Frances M. Ross,¹ D and R. Jaramillo^{1,a)} D

AFFILIATIONS

- Department of Materials Science and Engineering, Massachusetts Institute of Technology, Cambridge, Massachusetts 02139
- ²MIT.nano, Massachusetts Institute of Technology, Cambridge, Massachusetts 02139
- ³2D Crystal Consortium, Materials Research Institute, Pennsylvania State University, University Park, Pennsylvania 16802
- Department of Physics, Pennsylvania State University, University Park, Pennsylvania 16802

Note: This paper is a part of the Special Topic Collection on Thin Film Deposition for Materials Discovery.

a)Author to whom correspondence should be addressed: rjaramil@mit.edu

ABSTRACT

We report the synthesis of large-area, high-Ti-content, $Mo_{1-x}Ti_xS_2$ alloy thin films in the 2H phase at temperature as low as 500 °C using a scalable two-step method of metal film deposition, followed by sulfurization in H_2S . Film processing at higher temperature accelerates Ti segregation, film coarsening, and the formation of TiS_2 in the 1T phase. Crystal growth at higher temperature results in the formation of multiple binary sulfide phases, in agreement with the equilibrium phase diagram. Making highly metastable, smooth, and uniform single-phase alloy films, therefore, hinges on developing low-temperature processing. Our results are relevant to the development of technologies based on designer transition metal dichalcogenide alloys, including in photonic integrated circuits and gas sensing.

Published under an exclusive license by the AVS. https://doi.org/10.1116/6.0002227

I. INTRODUCTION

Transition metal dichalcogenides (TMDs) feature strong light-matter interaction and intriguing isomerism (i.e., competing phases with strongly contrasting optical properties) that suggests applications as phase-change materials for optical phase control in photonic integrated circuits (PICs). Alloy designs involving multiple metals offer a path toward new and useful TMDs that combine the relatively low optical loss in the near infrared of many sulfide TMDs, with lower energy requirements for phase-change functionality than in pure sulfides (e.g., MoS₂). 1,2

There has been substantial research into isomorphous TMD alloys, such as the Mo-W-S-Se system that crystallizes in the trigonal 2H phase (MoS₂ structure type). The polymorphous system Mo-W-Te featuring 2H, 1T', and T_d phases has been well studied, motivated in part because the phase transformations change electronic topology. Most other polymorphous systems are far less understood. The vast number of polymorphous TMD alloy systems

could include many materials useful for their phase-change, catalytic, and energy-storage properties. Results of theoretical modeling, and synthesis of powders and nanocrystals, demonstrate the interest and potential of isomorphous TMD alloys. The work here addresses a need for progress in thin film processing.

We report the synthesis of $\mathrm{Mo_{1-x}Ti_x}S_2$ thin films using a two-step method of metal film deposition by magnetron sputtering, followed by sulfurization in $\mathrm{H_2S}$ in a hot-wall tube furnace. The method is highly repeatable and compatible with wafer-scale deposition. Our approach differs from more widely used solid-source chemical vapor transport (CVT) methods to synthesize TMD thin films. Solid-source CVT is productive for research, but is difficult to scale: powder precursors become poisoned and depleted, and the mass transport and reaction kinetics present challenges to controlling crystal nucleation and growth on a wafer scale. Gas-source chemical vapor deposition (including metal-organic chemical vapor deposition) is desirable for future manufacturing of

microelectronic and optoelectronic technologies, but is likely too slow and expensive for many applications. 12 Our two-step method is based on physical vapor deposition (PVD) and chalcogenide conversion in H₂S gas, both of which processes are relatively fast and industrially scalable. H2S is corrosive and toxic and must be handled with appropriate safety precautions, but it is not unlike other gases routinely used in semiconductor manufacturing today.

We focus on a fundamental challenge of alloy design: making uniform materials of a desired composition and phase while suppressing chemical segregation and formation of unwanted secondary phases. We emphasize relatively low sulfurization temperature, as low as 500 °C, which slows phase segregation and is compatible with deposition on PIC wafers including waveguides and dielectrics. Low processing temperature also promotes smooth and uniform films, which are needed for planar device processing. We design for relatively thick (over 10 nm) and nanocrystalline films. The film thickness, much larger than monolayer and few-layer films that are emphasized for TMD optoelectronics and microelectronics, is chosen to enhance the optical interaction volume in PIC devices, as we have demonstrated through numerical simulation.¹³ We claim that nanocrystalline, dense films may be preferable to single-crystal films for phase-change functionality in PIC applications: grain boundaries make a much smaller contribution to parasitic, below-bandgap optical loss than do chemical impurities, and nanocrystalline material may have lower barriers to phase-change behavior than single crystals, as has been discussed for phase transformations in other classes materials. 14-16 The nanocrystalline, vertically far-from-equilibrium thin films enabled by our two-step process may prove useful also for applications in chemical sensing and catalysis.

II. EXPERIMENT

We use a two-step method to synthesize Mo_{1-x}Ti_xS₂ films. First, we deposit precursor Mo-Ti alloy films, of thickness below 10 nm, by magnetron sputtering (AJA international Orion 5, Ar gas, base pressure 10^{-5} Torr, process pressure 10^{-3} Torr, Mo gun power: 30-40 W, Ti power: 50-60 W) on Si₃N₄/Si substrates. We choose Si₃N₄ as a substrate relevant for PIC device integration, and to avoid oxide substrates that could be a source of oxygen during sulfurization. Our substrate size is usually less than $20 \times 100 \text{ mm}^2$, limited by our furnace tube diameter 38 mm and quartz sample holder size $30 \times 120 \text{ mm}^2$. The substrates are rinsed with isopropyl alcohol before metal deposition.

When depositing the Mo-Ti precursor films, we control the composition by calibrating the metal source rates, using a quartz crystal microbalance (QCM) before deposition by co-sputtering. The ratio of Mo:Ti metals determined by QCM calibration is subject to systematic errors, including that we calibrate the QCM for Ti metal, but Ti is likely to partially oxidize, even in the sputtering chamber. We measure the ratio of metals again after film sulfurization, by energy dispersive x-ray spectroscopy (EDS). Therefore, throughout this paper, we label our samples according to the metal composition x (as in $Mo_{1-x}Ti_xS_2$) according to QCM calibration, unless explicitly stated otherwise. Although Ti and Mo metals have a wide miscibility gap, we assume that they are fully mixed in the precursor films, which are deposited on unheated substrates.1

We sulfurize the precursor films in a hot-wall tube furnace reactor at atmospheric pressure, in a flow of between 20-100 SCCM H₂S and 0-200 SCCM forming gas (5% H₂, 95% N₂), at temperature between 500 and 600 °C. We use two different methods to cool the samples after sulfurization. "Slow cooling" refers to simply turning off the heating elements, and allowing the furnace to cool on its own, whereas "quench cooling" refers to opening the furnace enclosure, directly exposing the full hot tube to ambient air. Slow cooling from 500 to 300 °C takes over 5 h, whereas this same temperature drop is achieved in seconds during quench cooling. In both methods, the H₂S environment is maintained during cooling to avoid oxidation. The resulting sulfurized films appear uniform across centimeter-scale substrates. All the reported film samples and their detailed growth condition are summarized in Table S1.11

We use x-ray photoelectron spectroscopy (XPS, Thermo Scientific Nexsa XPS, Al K α source) to characterize the surface composition and chemistry of our films. We determine phase using Raman spectroscopy (Renishaw Invia Reflex Micro Raman), with an excitation wavelength of 532 nm. We use atomic force microscopy (AFM, Veeco Dimension 3100) to characterize film morphology. We perform scanning electron microscopy (SEM, Zeiss Merlin) in plan-view geometry. We perform atomic resolution scanning transmission electron microscopy (STEM) in cross sectional geometry. We prepare lamellar cross sections for STEM imaging using a focused ion beam (FEI Helios 600) system, with Au and Pt protection layers. We image samples using a probecorrected microscope (Thermo Fisher Scientific Themis Z G3 60-300 kV S/TEM) operated at 200 kV with a beam current of 20-40 pA, and 19.6 mrad convergence angle, as well as a field-emission JEOL 2010F TEM operated at 200 kV. We collect 4D STEM data in microprobe STEM mode using an electron microscope pixel array detector, with a convergence angle of 0.48 mrad and an exposure time of 1 ms. We process the 4D STEM data with the software PY4DSTEM. 19 We characterize film optical properties using spectroscopic ellipsometry (SE, Semilab SE2000).

To examine the thermodynamic stability of Mo_{0.5}Ti_{0.5}S₂, we attempted polycrystalline synthesis using the solid-state reaction method, and single crystal growth using the horizontal flux growth method. For polycrystalline synthesis, we heated stoichiometric mixtures of high-purity Ti, Mo, and S powders in an evacuated quartz tube to 1000 °C and held it at this temperature for 8 days, then allowed the furnace to cool uncontrolled. We characterized the resulting powder by x-ray diffraction (XRD). We then ground the precompounded polycrystals into a fine powder, pressed this into a 10 mm diameter pellet, and used this pellet as the precursor for crystal growth. We transferred the pellet into an evacuated 10 cm long, 13 mm inner diameter quartz tube, together with 10 g of NaCl-CsCl eutectic mixture (molar ratio of 38:62). We performed all sample preparation steps (except for pellet preparation—it seems likely that the sample experienced some oxidation during this step, as discussed with the XRD results below) in an argon-filled glovebox to minimize oxidation. We placed the sealed ampoule in a two-zone horizontal tube furnace, with the precursor placed at the hot end at 1100 °C, and a temperature gradient of 50 °C to the cold end (at 1050 °C), and held for 10 days. We then cooled the ampoule to 850 °C over 100 h, followed by another 100 h to

650 °C. Finally, the furnace was naturally cooled to room temperature, and we observed many dark silver crystals near the cold end. After washing in de-ionized water and then with acetone, we found as-grown, plate-like crystals of submillimeter size. We selected and ground multiple crystals into powder to enable phase identification by XRD. We performed XRD using a Malvern Panalytical Empyrean with Cu- $K_{\alpha 1}$ radiation. The XRD data were analyzed using Rietveld refinement (x'PERT HIGHSCORE PLUS software) to identify the phases. The parameters refined were scaling factor, background, vertical specimen displacement, lattice parameters, atomic positions, preferred orientation, and Caglioti halfwidth W, as shown in Table S2. ¹⁸

III. RESULTS AND DISCUSSION

In Fig. 1, we present a $Mo_{0.6}Ti_{0.4}S_2$ film sulfurized at 550 °C for 1 h, in 50 SCCM H_2S and 150 SCCM forming gas. Micrographs

reveal a dense, nanocrystalline film, decorated by protruding, iso-lated particles. The film is a uniform TMD alloy, and the particles are titanium oxide. The precursor film was 5 nm thick, and the sulfurized film is 17 nm thick, consistent with the factor of 3.36 (3.26) thickness expansion expected for converting a Mo (Ti) metal film to MoS₂ (TiS₂); the film roughness is 2.1 nm, as measured by AFM. The TMD alloy is Mo-rich, relative to the precursor, due to the segregation of Ti in the particles on the surface. XPS data [Fig. 1(d), measured after 30 s ion milling] suggest that both Mo and Ti in the film are fully sulfurized and is consistent with core-level spectroscopy on MoS₂ and TiS₂. Depth-profiling reveals that the fraction of oxidized Ti increases near the surface, consistent with a sulfide Mo_{1-x}Ti_xS₂ film, and TiO_x particles that sit on top of the film.

We use a combination of STEM EDS, atomic-resolution imaging, and Raman spectroscopy to identify the composition and phase of the continuous film. In Fig. 2(a), we present high-angle annular dark field (HAADF) imaging and EDS data, further

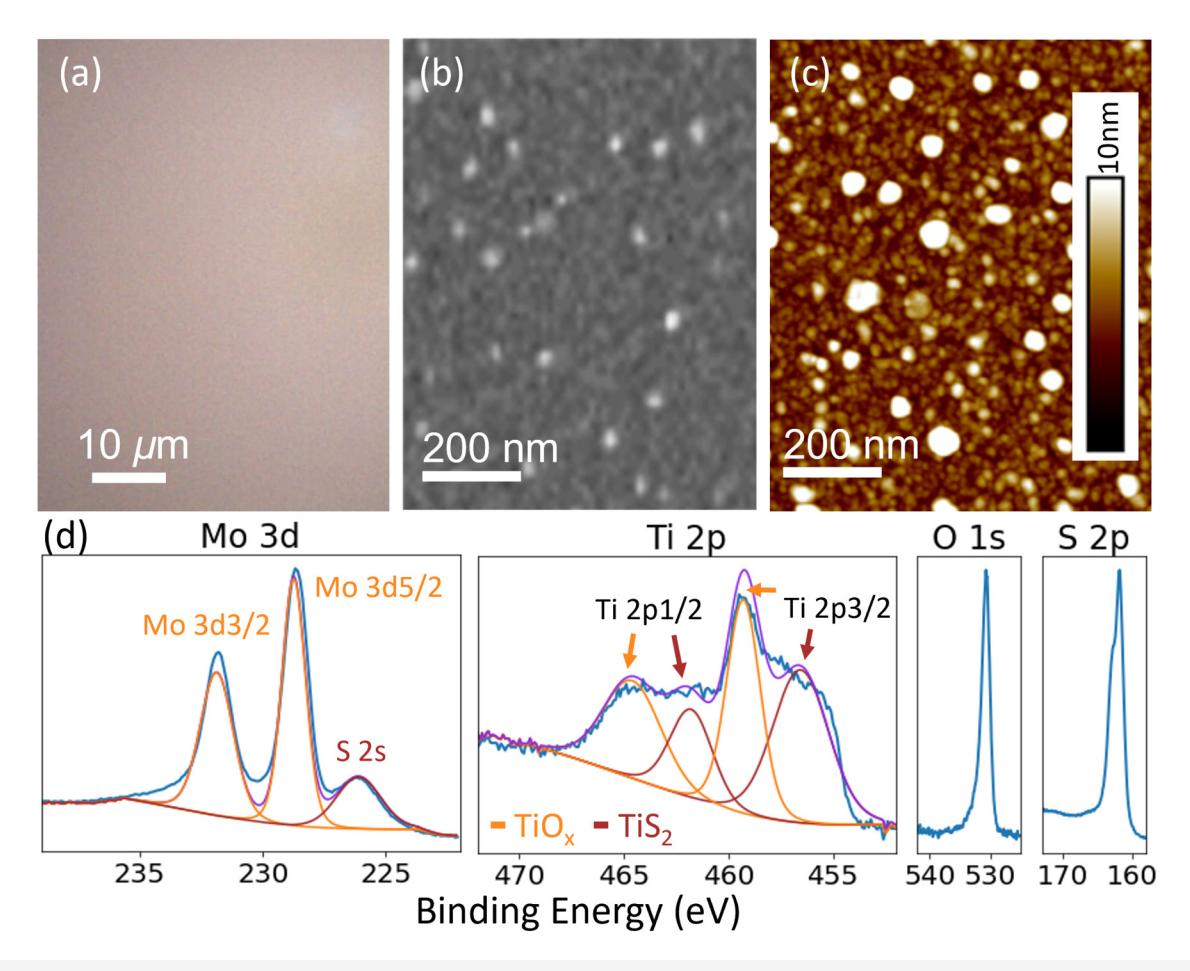


FIG. 1. $Mo_{0.6}$ Ti_{0.4}S₂ film, 17 nm thick, synthesized by sulfurization at 550 °C for 1 h. (a)–(c) Optical, SEM, and AFM micrographs, showing a film-and-particle morphology. (d) XPS data measured after ion milling. We fit the Mo 3d spectrum with double peaks at 228.7 and 231.9 eV corresponding to Mo sulfide and single peak at 226.1 eV corresponds to S 2s. We fit the Ti 2p spectrum with two pairs of peaks: the pair at 464.6 and 459.3 eV corresponding to Ti oxide, and the pair at 461.8 and 456.5 eV corresponds to Ti sulfide.

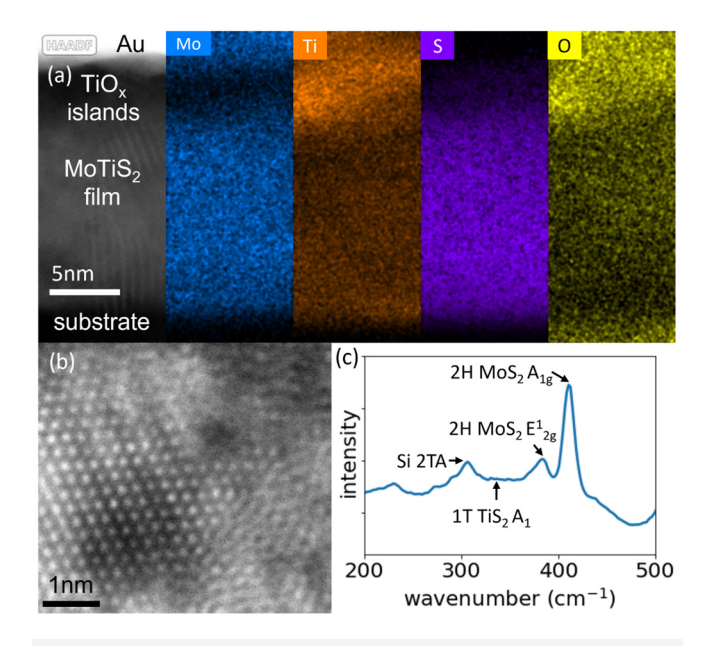


FIG. 2. Composition and phase analysis of the ${\rm Mo_{06}Ti_{0.4}S_2}$ film presented in Fig. 1. (a) Cross section HAADF micrograph and EDS maps. (b) HAADF STEM image collected at 200 kV. (c) Raman spectrum, with characteristic peaks labeled.

illustrating that the sample structure is a sulfide alloy film with (mostly isolated) TiO_x particles sitting on top. At the magnification of the images in Fig. 2(a), it is not apparent that the particles are isolated; this is clearer in lower-magnification data (Fig. S4). 18 EDS data are consistent with a Mo-rich film compared to the precursor composition, due to Ti segregation in the particles. The EDS data show an alloy film, with composition that varies through the film thickness: the Ti concentration decreases near the top, consistent with diffusion of Ti toward the particles (Fig. S1). EDS data show no indication of Ti- or Mo-rich secondary phase segregation within the film. The film composition cannot be fully quantified by EDS due to the overlap between Mo-L and S-K edges (Fig. S2). However, EDS quantification using only the Mo K-edge indicates an average Mo:Ti ratio of 70:30 (varying from 63:37 to 73:27 from bottom to top). Atomic-resolution imaging [Fig. 2(b)] shows a triangular lattice, consistent with a layered crystal structure and hexagonal symmetry; definitive phase identification by TEM is difficult due to the nanocrystalline, irregular film texture, however scanning electron diffraction (4D STEM, below) also attests to the 2H phase. Raman data [Fig. 2(c)] display the peaks at 383 and 411 cm⁻¹, typical of 2H-MoS₂. The peak at 335 cm⁻¹ typical of 1T-TiS₂ is not observed (the peak at 305 cm⁻¹ is 2TA scattering from the substrate). 20 We conclude that the continuous film is $Mo_{0.7}Ti_{0.3}S_2$ in the 2H, trigonal phase (MoS₂ structure type).

To investigate the mechanism of particle formation, we sulfurize films for varying temperature, time, and cooling rate. Our previously calculated Gibbs free energy-composition data predict that the MoS₂-TiS₂ binary system is fully immiscible at moderate temperature and that the phase composition at thermodynamic

equilibrium is segregated 2H-MoS₂ and 1T-TiS₂. We therefore expect a thermodynamic driving force for Ti and Mo to segregate during sulfurization and that increased time-temperature processing (i.e., longer time and/or higher temperature) will promote mass segregation and crystallization of the 2H and 1T phases. We see this expectation borne out in the experiment. In Figs. 3(a) and 3(b), we present SEM data for $Mo_{0.5}Ti_{0.5}S_2$ sulfurized at 500 °C (36 h) and 600 °C (2 h); both were cooled slowly. Both samples show a substantial quantity of particles segregated at the film surface. Based on other results presented here, we conclude that these particles are Ti-rich. The particles in the 600 °C sample have undergone substantial coarsening, compared to the 500 °C sample. This suggests a process of nucleation and growth, rate-limited by thermally activated diffusion. We conclude that the Ti diffusion length is longer at 600 °C and 2 h than at 500 °C and 36 h. By counter-varying the time and temperature, we are able to extract a lower bound of 1.68 eV for the activation energy for Ti diffusion. We are not aware of previously published results on Ti diffusion in chalcogenides with which this number can be directly compared; Ti cation diffusion in titanomagnetite solid solutions (i.e., oxides) was determined to have an activation energy of 2.58 eV.²¹ Raman data [Fig. 3(c)] show that sulfurization at 600 °C results in the formation of the 1T-TiS2 phase, whereas this phase is not detected in the sample sulfurized at 500 °C. EDS mapping (Fig. S3) demonstrates that sulfurization at 500 °C results in particles rich in Ti and O, suggestive of incomplete transformation to TiS₂.

The data in Figs. 3(a)-3(c) are consistent with a picture of thermally activated Ti segregation and 1T-TiS $_2$ crystallization. The process of phase segregation occurs first by Ti metal diffusion and coalescence into Ti-rich particles, which then transform into TiS $_2$ if allowed sufficient time and temperature in the sulfurizing atmosphere. Since MoS $_2$ forms from Mo metal more readily than TiS $_2$ does from Ti metal (due in part to residual oxygen), it seems likely that during sulfurization, Ti metal and α -TiO $_x$ diffuse through MoS $_2$.

The mechanism suggests that suppressing the phase segregation by rapid sulfurization at low temperature is key to making high-Ti-content, single-phase Mo_{1-x}Ti_xS₂ films. Lower temperature slows down both metal segregation and sulfurization reactions, requiring a balance to optimize the process outcome. We find that sulfurization at 550 °C for 1 h followed by quench cooling yields a substantial improvement over the higher-temperature and/or longertime processes reported in Figs. 3(a)-3(c). In Figs. 3(d)-3(f), we present the results of sulfurizing films with two very different Ti contents, $Mo_{0.8}Ti_{0.2}$ and $Mo_{0.4}Ti_{0.6}$, with these processing conditions. The resulting films (also see the Mo_{0.6}Ti_{0.4}S₂ sample reported above) are much smoother, and the Raman spectra show evidence of only the 2H phase. We conclude that faster and lower-temperature processing can successfully trap Ti during sulfurization, yielding far-from-equilibrium, high-Ti-content 2H-phase thin films. We hypothesize that the slight blue shift of the A_{1g} Raman peak for $Mo_{0.8}Ti_{0.2}S_2$ relative to $Mo_{0.4}Ti_{0.6}S_2$ [Fig. 3(f)] may result from the different film composition.

The results of single-crystal synthesis experiments further highlight the importance of relatively rapid and low-temperature sulfurization to stabilize high-Ti-content $2H-(Mo,Ti)S_2$ alloys. In Fig. 4(a), we present XRD data measured on a powder sample

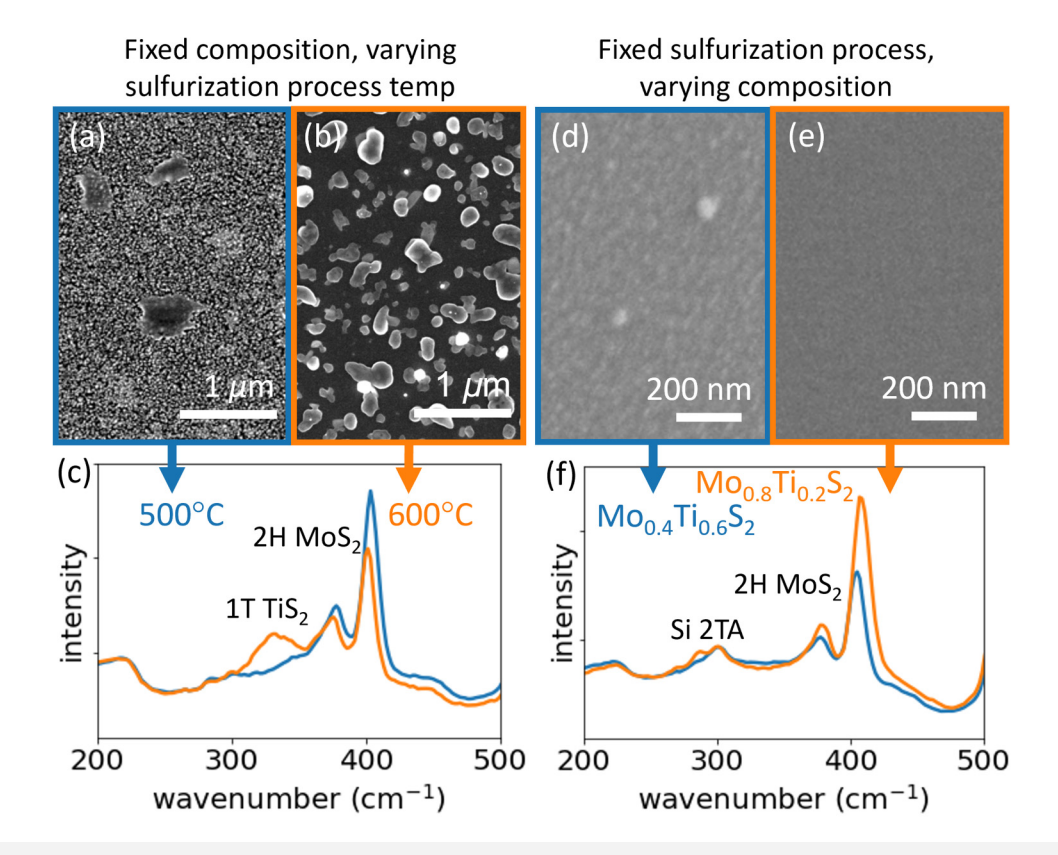


FIG. 3. Examples of how film morphology and phase vary with sulfurization temperature, time, cooling rate, and precursor composition. [(a) and (b)] Plan-view SEM micrographs of $Mo_{0.5}Ti_{0.5}S_2$ films sulfurized at 500 °C (36 h) and 600 °C (2 h), respectively, both with slow cooling. (c) Raman spectra of films shown in (a) and (b), illustrating the emergence of 1T-TiS₂ phase with higher-temperature sulfurization. [(d) and (e)] Plan-view SEM micrographs of $Mo_{0.4}Ti_{0.6}S_2$ and $Mo_{0.8}Ti_{0.2}S_2$ films, respectively, both sulfurized at 550 °C (1 h) with quench cooling. (f) Raman spectra of films shown in (d) and (e), illustrating the presence of only 2H phase for films sulfurized at 550 °C and for shorter time, even as the Ti content triples from 20% to 60% on metals basis.

obtained via grinding the crystals that were grown using the horizontal flux method, with a growth temperature window of 1100-1050 °C and a growth period of 10 days. From Rietveld refinement, we find that, while the nominal composition of the source material used for crystal growth is Mo_{0.5}Ti_{0.5}S₂, the resulting sample does not contain such an alloy; instead, it includes several binary phases, i.e., MoS₂, Ti_{1.083}S₂, TiS₃, and TiO₂ (full refinement details presented in Table S2).¹⁸ In Fig. 4(b), we reproduce the previously reported phase diagram of the Mo-Ti-S ternary system for 1300 °C (the only temperature for which a phase diagram is available).²² The binary phases identified in our sample can be understood in terms of this phase diagram. TiS₂ is unstable above approximately 1000 °C, whereupon it decomposes into one of many sulfurdeficient phases.²³ The Ti_{1.083}S₂ phase (ICDD: 01-084-0372, P-3m1, trigonal) identified in our analyses is one of those sulfurdeficient, layered titanium sulfides. During the high-temperature reaction, we expect segregation of titanium sulfide, MoS2, and sulfur vapor. Further, we hypothesize that, upon cooling from the growth temperature, the binary sulfide partially reacts with condensing sulfur vapor, forming the sulfur-rich phase TiS3. Powder polycrystalline samples made by the solid-state reaction method had a similar phase composition (Fig. S5). 18 The results of these bulk synthesis experiments further illustrate that (Mo,Ti)S₂ is a thermodynamically unstable alloy and that its synthesis requires kinetic control.

In Fig. 5, we present results of 4D STEM measurements of a $Mo_{0.6}Ti_{0.4}S_2$ film sulfurized at 550 °C for 1 h, with quench cooling. Figure 5(a) illustrates diffraction data measured at a single pixel within the film. We see a pair of low-angle diffraction spots, at a radius of $(6.44 \pm 0.7 \text{ Å})^{-1}$, corresponding to the layer spacing. Their appearance as discrete spots indicates that the crystal layers are aligned vertically with respect to the substrate. The large uncertainty in the layer spacing estimate is the instrument response function under these measurement conditions. In Fig. 5(b), we present the analysis of the angular distribution of diffraction intensity averaged across 60×256 pixels, spanning an area of $15 \times 64 \text{ nm}^2$. The data show that the film is strongly textured with the layers aligned vertically. In other words, the single-spot analysis in Fig. 5(a) is representative of the film as a whole.

The far-from-equilibrium TMD alloy films demonstrated here could be useful for various applications, including photonic integrated circuits, for which they could be deposited and patterned

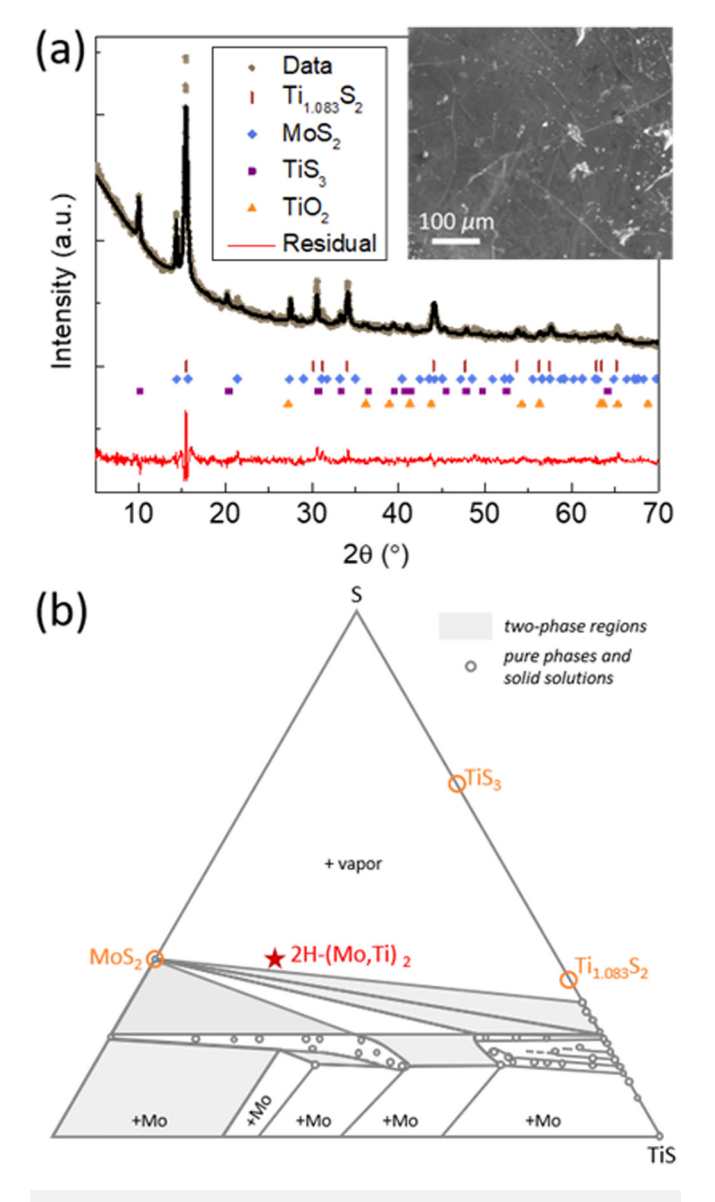


FIG. 4. Attempt to synthesize $Mo_{0.5}Ti_{0.5}S_2$ by high-temperature horizontal flux growth results in phase segregation into binary sulfides. (a) XRD data measured on a powder sample, which was obtained via grinding flux-grown crystals (gray symbols); the Rietveld refinement (black curve) identified phases present (colored symbols). The red curve is the difference between the experimental and fitted diffraction patterns. (Inset) SEM micrograph of flux-grown single crystal. (b) Equilibrium phase diagram at 1300 °C; data are taken from the work of Wada and Onoda (Ref. 22). Orange circles indicate the phases identified in our sample. The red star indicates the approximate composition of the metastable, high-Ti-content alloy thin films reported here. (Color online).

into devices to control the optical phase. In anticipation of future such developments, we report in Fig. 6 the optical properties of a Mo_{0.6}Ti_{0.4}S₂ film sulfurized at 550 °C for 1 h, with quench cooling (as in Fig. 5), measured by SE. In Fig. 6(a), we present the

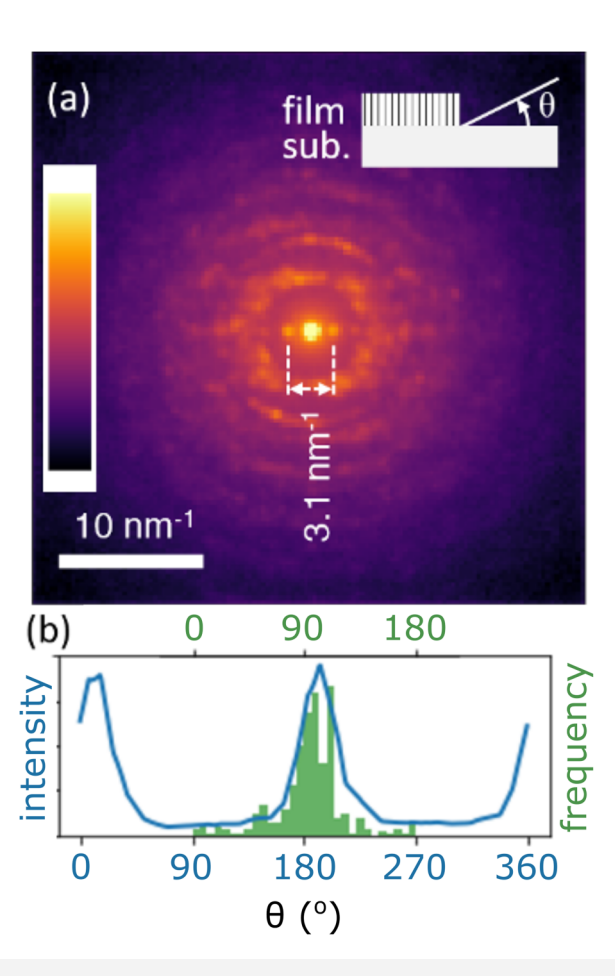


FIG. 5. 4D STEM diffraction data measured on $Mo_{0.6}Ti_{0.4}S_2$ films synthesized at 550 °C for 1 h with quench cooling. (a) Diffraction data measured at a spot within the TMD film. The vertical direction in the image corresponds to the out-of-plane direction in the sample. Color bar indicates diffraction intensity on a log scale. The two spots at low angle correspond to a layer spacing of 0.644 nm, close to the layer spacing of MoS₂ (0.615 nm) and TiS₂ (0.569 nm). Their appearance as discrete spots, instead of a ring, indicates that the film is strongly textured with the TMD layers vertical, as illustrated in the inset. (b) Solid blue curve, bottom axis: angular distribution of diffraction intensity at radius (0.644 nm)⁻¹ (within an annulus one pixel wide in the 4D STEM data set) averaging data measured at 60×256 pixels across a film cross section of area $15 \times 64 \,\mathrm{nm^2}$. The prominent central peak indicates that the film texture, visualized in (a) for measurement at a small region of area $2.5 \times 4\,\text{nm}^2$, is representative of the film as a whole. Green bars, top axis: histogram of the angle between TMD layer and substrate, for every $1\times 1\,\mathrm{nm}^2$ spot through the film cross section. The layers are preferentially aligned vertically, with an angular spread of 27° (root-mean-square) around the mean (94°). (Color online).

measured spectroscopic angles, Ψ and Δ . In Fig. 6(b), we present the inferred, effective complex refractive indices, $n_{\rm eff}$ and $k_{\rm eff}$, and compare with results for MoS₂. TMDs are strongly birefringent, and the film texture means that our SE measurements mix the ordinary and extraordinary components of the refractive index, hence the label "effective." Meanwhile, the data we present for MoS₂ are the ordinary and extraordinary refractive indices.²⁴

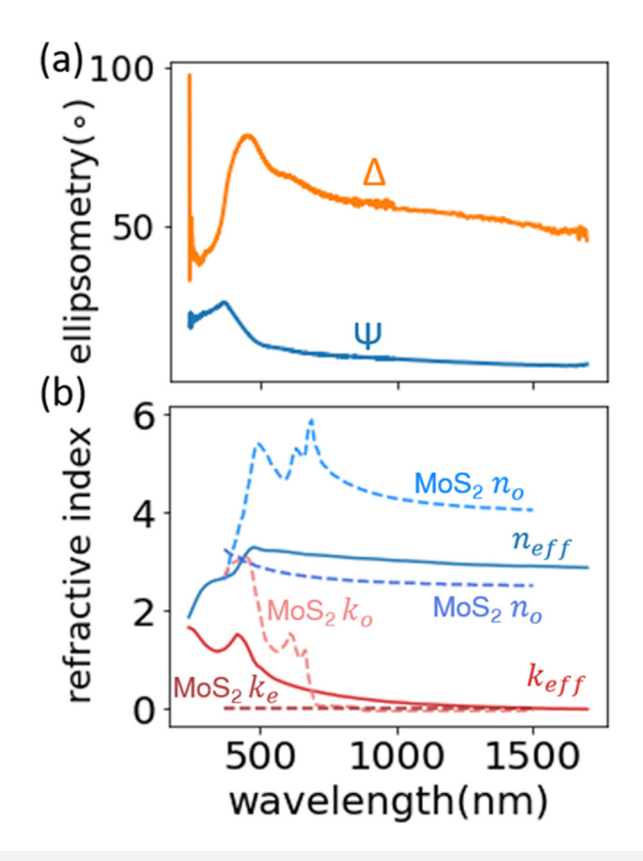


FIG. 6. SE results for Mo_{0.6}Ti_{0.4}S₂ films, sulfurized at 550 °C for 1 h with quench cooling. (a) Ψ and Δ spectra measured at a 75° angle of incidence. (b) Effective refractive indices $n_{\rm eff}$ and $k_{\rm eff}$; data are labeled effective because measurements mix the ordinary and extraordinary components, due to the film texture. Also shown for reference are the ordinary and extraordinary refractive indices of MoS₂ (Ref. 24).

We observe one discrete absorption resonance in the $Mo_{0.6}Ti_{0.4}S_2$ film, at 420 nm (2.95 eV). The peak position is close to resonances in 2H-MoS₂ at 2.8 and 3.1 eV, but the specific origin is unknown.²⁵⁻²⁷ The multiple absorption resonances in 2H-MoS₂ may also be present in our film, but smoothed due to structural disorder. Due to the film texture with vertical layer orientation, the measured k_{eff} likely depends most on the extraordinary component, which in pure 2H-MoS2 has no absorption resonance in this energy range. The k_{eff} data show that $Mo_{0.6}Ti_{0.4}S_2$ has low optical loss below the bandgap, comparable to pure MoS₂, despite the high concentration of Ti which would be expected to favor metallicity.

IV. SUMMARY AND CONCLUSIONS

We synthesized large-area, high-Ti-content, single-phase 2H alloy Mo_{1-x}Ti_xS₂ thin films via a two-step method with sulfurization temperature as low as 500 °C. Since the high-Ti-content alloys Mo_{1-x}Ti_xS₂ are far-from-equilibrium in the MoS₂-TiS₂ binary system, there is a thermodynamic driving force to segregate Ti and Mo during sulfurization. We suggest that phase segregation occurs first by the diffusion of Ti metal and/or TiO_x oxide to the film surface, where they coalesce into Ti-rich particles that emerge from the sulfurization process as TiOx or TiS2, depending on the extent of sulfurization. Crystal growth at elevated temperature results in the formation of Mo and Ti binary sulfides, consistent with the equilibrium phase diagram. Rapid sulfurization at lower temperature is key to suppressing phase segregation and making smooth and uniform alloy films, by kinetically trapping Ti in the forming TMD crystal structure. Based on the trends that we report here, we expect that the film morphology could be further improved by more precise control of the sulfurization and cooling time (e.g., rapid thermal annealing) and by further reducing the background O2 concentration in the reactor, as discussed in our previous work on TiS₂.

The 2H-Mo_{1-x}Ti_xS₂ alloy films exhibit low sub-bandgap optical loss, despite a large concentration of Ti, which ought to favor metallicity (TiS2 is semimetallic). This is promising for using these alloys for optical phase control with low insertion loss in photonic integrated circuits. 13 By approaching the 2H-1T phase boundary in metastable alloys, we expect to reduce the thermodynamic barrier for phase transformation, enabling phase-change functionality in TMD alloys. We also note that the nanocrystalline and vertically aligned film texture may be useful for applications in chemical sensing and catalysis.

ACKNOWLEDGMENTS

This work was supported by an Office of Naval Research MURI through Grant No. N00014-17-1-2661. We acknowledge the use of facilities and instrumentation supported by NSF through the Massachusetts Institute of Technology Materials Research Science and Engineering Center under No. DMR-1419807. This work was performed in part at the Harvard University Center for Nanoscale Systems (CNS), a member of the National Nanotechnology Coordinated Infrastructure Network (NNCI), which is supported by the National Science Foundation under NSF Award No. 1541959. This work was performed in part in the MIT.nano Characterization Facilities. The bulk single crystal growth work was performed at the Pennsylvania State University Two-Dimensional Crystal Consortium-Materials Innovation Platform (2DCC-MIP), which is supported by NSF under Cooperative Agreement Nos. DMR-1539916 and DMR-2039351. K.R. acknowledges funding and support from an MIT MathWorks Engineering Fellowship and ExxonMobil Research and Engineering Company through the MIT Energy Initiative. We thank Colin Ophus for useful discussions on the utilization of PY4DSTEM package.

AUTHOR DECLARATIONS

Conflict of Interest

The authors have no conflicts to disclose.

Author Contributions

Yifei Li: Conceptualization (equal); Data curation (equal); Formal analysis (equal); Investigation (equal); Methodology (equal); Software (equal); Visualization (equal); Writing - original draft (equal); Writing - review & editing (equal). Kate Reidy: Data curation (equal); Formal analysis (equal); Investigation (equal);

Methodology (equal); Visualization (equal); Writing - review & editing (equal). Aubrey Penn: Data curation (equal); Investigation (equal); Methodology (equal). Seng Huat Lee: Data curation (equal); Formal analysis (equal); Investigation (equal); Methodology (equal); Resources (equal); Writing - review & editing (equal). Baoming Wang: Investigation (equal); Methodology (equal). Kevin Ye: Data curation (equal); Formal analysis (equal); Visualization (equal). Zhiqiang Mao: Data curation (equal); Formal analysis (equal); Investigation (equal); Methodology (equal); Project administration (equal); Resources (equal); Supervision (equal); Writing review & editing (equal). Frances M. Ross: Funding acquisition (equal); Investigation (equal); Methodology (equal); Project administration (equal); Resources (equal); Supervision (equal); Writing review & editing (equal). R. Jaramillo: Conceptualization (equal); Data curation (equal); Formal analysis (equal); Funding acquisition (equal); Investigation (equal); Methodology (equal); Project administration (equal); Resources (equal); Supervision (equal); Visualization (equal); Writing - original draft (equal); Writing - review & editing (equal).

DATA AVAILABILITY

The data that support the findings of this study are available from the corresponding author upon reasonable request.

REFERENCES

- ¹A. Singh, S. S. Jo, Y. Li, C. Wu, M. Li, and R. Jaramillo, ACS Photonics 7, 3270 (2020).
- ²A. Singh, Y. Li, B. Fodor, L. Makai, J. Zhou, H. Xu, A. Akey, J. Li, and R. Jaramillo, Appl. Phys. Lett. 115, 161902 (2019).
- ³R. Lv, H. Terrones, A. L. Elías, N. Perea-López, H. R. Gutiérrez, E. Cruz-Silva, L. P. Rajukumar, M. S. Dresselhaus, and M. Terrones, Nano Today 10, 559 (2015).
- ⁴S. M. Oliver et al., 2D Mater. 4, 045008 (2017).
- ⁵Z. Hemmat et al., Adv. Mater. 32, 1907041 (2020).

- ⁶C. Linderälv, J. M. Rahm, and P. Erhart, Chem. Mater. 34, 9364 (2022).
- ⁷Z. Du et al., Nature 577, 492 (2020).
- ⁸S. S. Jo, Y. Li, A. Singh, A. Kumar, S. Frisone, J. M. LeBeau, and R. Jaramillo, J. Vac. Sci. Technol. A 38, 013405 (2020).
- ⁹Y. Li, A. Singh, K. Reidy, S. S. Jo, F. M. Ross, and R. Jaramillo, Adv. Funct. Mater. **30**, 2003617 (2020).
- ¹⁰J. Zhou et al., Nature **556**, 355 (2018).
- ¹¹T. Kang, T. W. Tang, B. Pan, H. Liu, K. Zhang, and Z. Luo, ACS Mater. Au 2, 665 (2022).
- 12T. H. Choudhury, X. Zhang, Z. Y. Al Balushi, M. Chubarov, and J. M. Redwing, Annu. Rev. Mater. Res. 50, 155 (2020).
- ¹³A. Singh, S. S. Jo, Y. Li, C. Wu, M. Li, and R. Jaramillo, ACS Photonics 7, 3270 (2020).
- ¹⁴D. Prabhu, A. Narayanasamy, K. Shinoda, B. Jeyadeven, J.-M. Greneche, and K. Chattopadhyay, J. Appl. Phys. **109**, 013532 (2011).
- ¹⁵M. H. Frey and D. A. Payne, Phys. Rev. B **54**, 3158 (1996).
- ¹⁶Q. Sun, A. Aslan, M. Li, and M. Chen, Sci. China Technol. Sci. 57, 671 (2014).
- 17T. B. Massalski and H. Okamoto, Binary Alloy Phase Diagrams, 2nd ed. (ASM International, Materials Park, OH, 1990).
- 18 See supplementary material at https://www.scitation.org/doi/suppl/10.1116/6.0002227 for a list of samples studied, further details on experimental methods, additional measurements of chemical composition and particle morphology, and XRD data and Rietveld refinement results.
- 19 B. H. Savitzky et al., Microsc. Microanal. 27, 712 (2021).
- ²⁰M. Ichimura, A. Usami, A. Wakahara, and A. Sasaki, J. Appl. Phys. 77, 5144 (1995).
- ²¹R. Aragon, R. H. McCallister, and H. R. Harrison, Contrib. Mineral. Petrol. 85, 174 (1984).
- ²²H. Wada and M. Onoda, J. Less Common Met. 135, 205 (1987).
- ²³B. Predel and O. Madelung, in *Group IV: Physical Chemistry* (Springer-Verlag, Berlin, 1998).
- ²⁴G. A. Ermolaev et al., Nat. Commun. 12, 854 (2021).
- ²⁵D. Y. Qiu, F. H. da Jornada, and S. G. Louie, Phys. Rev. Lett. **111**, 216805 (2013)
- ²⁶S. C. Bayliss and W. Y. Liang, J. Phys. C: Solid State Phys. 15, 1283 (1982).
- ²⁷A. Molina-Sánchez, D. Sangalli, K. Hummer, A. Marini, and L. Wirtz, Phys. Rev. B **88**, 045412 (2013).